Incremental Length Diffraction Coefficients for the Shadow Boundary of a Convex Cylinder

Thorkild B. Hansen, *Member, IEEE*, and Robert A. Shore, *Senior Member, IEEE*

***Abstract*—Incremental length diffraction coefficients (ILDC's) are obtained for the shadow boundaries of perfectly electrically conducting (PEC) convex cylinders of general cross section. A two-step procedure is used. First, the nonuniform (NU) current in the vicinity of the shadow boundary is approximated using Fock functions. The product of the approximated current and the free-space Green's function is then integrated on a differential strip of the cylinder surface transverse to the shadow boundary to obtain the ILDC's. This integration is performed in closed form by employing quadratic polynomial approximations for the amplitude and unwrapped phase of the integrand. Examples are given of both the current approximations and the integration procedure. Finally, as an example, the scattered far field of a PEC sphere is obtained by adding the integral of the NU ILDC's of a circular cylinder along the shadow boundary of the sphere to the physical optics (PO) far field of the sphere. This correction to the PO field is shown to significantly improve upon the accuracy of the PO far-field approximation to the total scattered field of the sphere.**

***Index Terms*—Physical theory of diffraction.**

I. Introduction

In the physical theory of diffraction (PTD) [1], the scattered field is divided into a physical optics (PO) field and a nonuniform (NU) field. The PO field for perfectly electrically conducting (PEC) objects is obtained from an integration of the PO current over the object. One reason for the limited accuracy of the PO field is that the PO current fails to closely approximate the exact current in the vicinity of shadow boundaries and on the shadow side. A significant improvement in the accuracy of the computed fields can, therefore, be obtained by finding good approximations for the fields radiated by the NU currents near the shadow boundary. Approximations for these NU fields can be obtained by first integrating the product of the free-space Green's function and the approximated NU current excited on a strip of differential width transverse to the shadow boundary of a canonical two-dimensional (2-D) scatterer that closely conforms locally to the shape of the actual scatterer in the vicinity of the shadow boundary. The differential fields obtained by this integration are known as the incremental length diffraction coefficients (ILDC's). Once the ILDC's are determined, the NU fields are obtained by integrating them along the shadow boundary of the actual scatterer.

Manuscript received April 6, 1998.

T. B. Hansen is with Schlumberger-Doll Research, Ridgefield, CT 06877 USA.

R. A. Shore is with the Air Force Research Laboratory/SNHA, Hanscom AFB, MA 01731 USA.

Publisher Item Identifier S 0018-926X(98)07494-8.

Although for some time ILDC's have been available for the shadow boundaries of 2-D PEC scatterers with sharp edges (such as the wedge [2]–[5]), it is only recently that they have been obtained for convex smoothly curved cylinders. Yaghjian *et al.* [6] obtain these ILDC's by approximating the fields radiated by the NU shadow-boundary currents of a general convex cylinder by the fields radiated by the NU shadow-boundary currents of circular cylinders and then substituting the approximated fields into general expressions [5]–[7]. These approximate ILDC's are then extended to account for a varying radius of curvature in the shadow region.

The purpose of this paper is to show how ILDC's can be obtained for the NU currents near the shadow boundaries of PEC 2-D convex cylinders of general cross section and smoothly varying radius of curvature by approximating and integrating the NU currents. We derive asymptotic expressions for the ILDC's that are rapidly calculable and usable in general-purpose computer codes. This method of obtaining convex-cylinder shadow-boundary ILDC's is an alternative to the field substitution of Yaghjian *et al.* [6] described above. The field substitution method, because it works directly with fields, is perhaps simpler than the method of this paper. For applications in which heightened accuracy is important, however, the NU current approximation and integration method described here may be preferable because it yields more accurate ILDC's than does the field substitution method [8].

In Section II, we give the Fock approximations of the NU currents on a convex cylinder for TE and TM oblique incidence. In Section III, we show how the ILDC's corresponding to the Fock NU current approximations can be obtained efficiently by using an accurate and rapidly calculable approximation to the radiation integral defining the ILDC. In Section IV, we show how to determine the canonical 2-D cylinders from the actual three-dimensional (3-D) scatterers. As an example of obtaining and using shadow-boundary ILDC's, we show results obtained for the field scattered by a PEC sphere illuminated by a plane wave.

II. Fock Currents on a Convex Cylinder

In this section, we give expressions for the Fock currents [9] on a convex perfectly conducting cylinder illuminated by an obliquely incident plane wave (see Fig. 1). Some of these results are available in the literature, for example [10], [11, pp. 83-86], [12]. We note, however, that the Fock currents in the illuminated region are given incorrectly in [10] and [12] and are not given in [11]; there are other errors as well. For this reason we derived all of the Fock currents for oblique

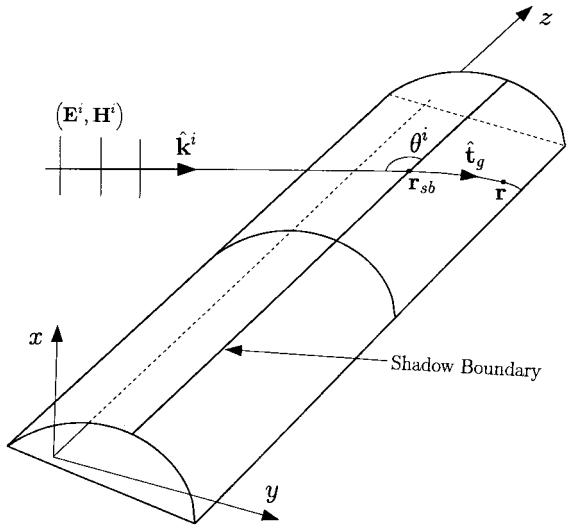

Fig. 1. Cross section of a convex cylinder with smoothly varying radius of curvature.

incidence from the expressions for normal incidence, using recently established relationships [13] between the currents excited by obliquely and normally incident plane waves. The details of these derivations can be found in [14]. In the following expressions for the Fock current approximations, the cylinder axis is parallel to z, and the unit normal vector for the cylinder surface is denoted $\hat{\mathbf{n}}$. The incident plane wave propagates in the direction $\hat{\mathbf{k}}^i$. An $e^{-i\omega t}$ time dependence is assumed with $\omega > 0$.

A. The Fock Current for TE Oblique Incidence

In this case, the incident electric and magnetic plane-wave fields are given by

$$\mathbf{E}^{\mathrm{TE},\,i}(\mathbf{r}) = -\,Z_0\hat{\phi}^i\, e^{i\mathbf{k}^i\cdot\mathbf{r}} \tag{1}$$

and

$$H^{\mathrm{TE},\,i}(\mathbf{r}) = -\,\hat{\theta}^i\, e^{i\mathbf{k}^i\cdot\mathbf{r}} \tag{2}$$

where Z_0 is the impedance of free-space, $\mathbf{k}^i = k\hat{\mathbf{k}}^i$ and $\hat{\mathbf{k}}^i = -\hat{\mathbf{x}}\sin\theta^i\cos\phi^i - \hat{\mathbf{y}}\sin\theta^i\sin\phi^i - \hat{\mathbf{z}}\cos\theta^i$ are the propagation direction of the incident plane wave, $\hat{\theta}^i$ and $\hat{\phi}^i$ are the spherical unit vectors corresponding to the direction (θ^i, ϕ^i), and $\mathbf{r} = x\hat{\mathbf{x}} + y\hat{\mathbf{y}} + z\hat{\mathbf{z}}$ denotes a general point.

In the illuminated region the Fock current approximation for the TE NU current is

$$\mathbf{K}^{\mathrm{TE},\,\mathrm{NU}}(\mathbf{r}) = \hat{\mathbf{n}}\times\mathbf{H}^{\mathrm{TE},\,i}(\mathbf{r})\,\widetilde{G}\left(\left[\frac{k\rho_g(\mathbf{r})}{2}\right]^{1/3}\hat{\mathbf{n}}\cdot\hat{\mathbf{k}}^i\right). \tag{3}$$

Here, $\widetilde{G}(x)$ is the modified Fock function defined as

$$\widetilde{G}(x) = G(x) - 2 \tag{4}$$

where $G(x) = e^{ix^3/3}g(x)$, with $g(x)$ being the Fock function defined in [15, pp. 63–64]. The radius of curvature of the generalized helical geodesic that forms an angle θ^i with the z axis is denoted $\rho_g(\mathbf{r})$ with

$$\rho_g(\mathbf{r}) = \frac{\rho_n(\mathbf{r})}{\sin^2\theta^i} \tag{5}$$

where $\rho_n(\mathbf{r})$ is the radius of curvature in the plane normal to the cylinder axis. The Fock current approximation for the TE total current is given by (3) with $\widetilde{G}(x)$ replaced by $G(x)$.

On the shadow side

$$\mathbf{K}^{\mathrm{TE}}(\mathbf{r}) = Y_0\,\hat{\mathbf{n}}_{sb}\cdot\mathbf{E}^{\mathrm{TE},\,i}(\mathbf{r}_{sb})\,e^{iks_g(\mathbf{r})}g(x_g)\left(\frac{\rho_g(\mathbf{r}_{sb})}{\rho_g(\mathbf{r})}\right)^{1/6}\hat{\mathbf{t}}_g. \tag{6}$$

In (6), $Y_0 = 1/Z_0$ is the free-space admittance, $\hat{\mathbf{n}}_{sb}$ is the normal to the cylinder at the shadow boundary point $\mathbf{r}_{sb}$, $s_g(\mathbf{r})$ is the distance along the geodesic on the cylinder from $\mathbf{r}_{sb}$ to $\mathbf{r}$, and $\hat{\mathbf{t}}_g$ is the tangent vector to the geodesic in the direction away from the shadow boundary. The quantity x_g is defined by

$$x_g = \left(\frac{k}{2}\right)^{1/3}\int_{\mathbf{r}_{sb}}^{\mathbf{r}}\frac{ds_g}{\rho_g(s_g)^{2/3}} \tag{7}$$

where the integration is performed along the geodesic that starts at $\mathbf{r}_{sb}$ and ends at the point $\mathbf{r}$ in the shadow region. For large distances from the shadow boundary the asymptotic form of the Fock function $g(x)$ [15, p. 64] can be used in (6) yielding the first creeping wave on the cylinder

$$\mathbf{K}^{\mathrm{TE}}(\mathbf{r}) \sim Y_0\,\hat{\mathbf{n}}_{sb}\cdot\mathbf{E}^{\mathrm{TE},\,i}(\mathbf{r}_{sb})\,e^{iks_g(\mathbf{r})}\frac{e^{\beta_1 x_g e^{5i\pi/6}}}{\beta_1 Ai(-\beta_1)} \cdot\left(\frac{\rho_g(\mathbf{r}_{sb})}{\rho_g(\mathbf{r})}\right)^{1/6}\hat{\mathbf{t}}_g \tag{8}$$

where β_1 is the negative of the first zero of the derivative of the Airy function.

B. The Fock Current for TM Oblique Incidence

In this case, the incident electric and magnetic plane-wave fields are given by

$$\mathbf{E}^{\mathrm{TM},i}(\mathbf{r}) = -\,\hat{\theta}^i\, e^{i\mathbf{k}^i\cdot\mathbf{r}} \tag{9}$$

and

$$\mathbf{H}^{\mathrm{TM},\,i}(\mathbf{r}) = Y_0\,\hat{\phi}^i\, e^{i\mathbf{k}^i\cdot\mathbf{r}}. \tag{10}$$

In the illuminated region, the Fock approximation for the TM NU current is

$$\mathbf{K}^{\mathrm{TM,NU}}(\mathbf{r}) = \hat{\mathbf{z}}K_z^{\mathrm{TM},\,\mathrm{NU}}(\mathbf{r}) = -\,i\,\hat{\mathbf{n}}\times\mathbf{H}^{\mathrm{TM},\,i}(\mathbf{r})\,\widetilde{F}\left(\left[\frac{k\rho_g(\mathbf{r})}{2}\right]^{1/3}\hat{\mathbf{n}}\cdot\hat{\mathbf{k}}^i\right) \cdot\left(\left[\frac{k\rho_g(\mathbf{r})}{2}\right]^{1/3}\hat{\mathbf{n}}\cdot\hat{\mathbf{k}}^i\right)^{-1} \tag{11}$$

or

$$K_z^{\mathrm{TM,NU}}(\mathbf{r}) = \frac{iY_0}{\sin^2\theta^i}\,\hat{\mathbf{z}}\cdot\mathbf{E}^{\mathrm{TM},i}(\mathbf{r})\,\widetilde{F}\left(\left[\frac{k\rho_g(\mathbf{r})}{2}\right]^{1/3}\hat{\mathbf{n}}\cdot\hat{\mathbf{k}}^i\right) \cdot\left[\frac{k\rho_g(\mathbf{r})}{2}\right]^{-1/3}. \tag{12}$$

In (11) and (12), $\widetilde{F}(x)$ is the modified Fock function defined as

$$\widetilde{F}(x) = F(x) - 2ix \tag{13}$$

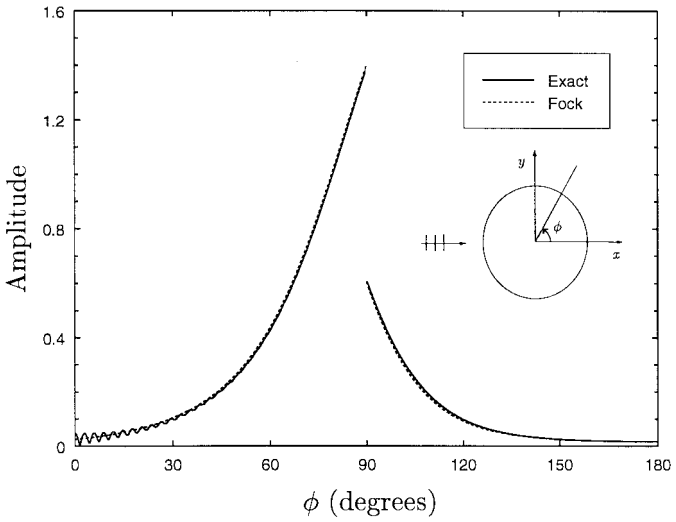

Fig. 2. Amplitude of $K_\phi^{\mathrm{TE,\,NU}}(a,\,\phi,\,z)$ for circular cylinder, $ka = 60$, $\phi^i = 180°$, $\theta^i = 90°$.

where $F(x) = e^{ix^3/3} f(x)$ and $f(x)$ is the Fock function defined in [15, pp. 63–64]. The Fock current approximation for the TM total current is given by (11) or (12) with $\widetilde{F}(x)$ replaced by $F(x)$.

On the shadow side of the cylinder, the Fock current is given by

$$K_z^{\mathrm{TM}}(\mathbf{r}) = if(x_g)e^{iks_g(\mathbf{r})}\,\frac{\hat{\mathbf{n}}_{sb}\cdot\mathbf{H}^{\mathrm{TM},i}(\mathbf{r}_{sb})}{\hat{\mathbf{n}}_{sb}\cdot\hat{\phi}^i\sin\theta^i}\left(\frac{\rho_g(\mathbf{r}_{sb})}{\rho_g(\mathbf{r})}\right)^{1/6} \cdot\left(\frac{k\rho_g(\mathbf{r})}{2}\right)^{-1/3} \tag{14}$$

where all quantities have been previously defined. For large distances from the shadow boundary the asymptotic form of $f(x)$ [15] can be used in (14) giving the first creeping wave on the convex cylinder

$$K_z^{\mathrm{TM}}(\mathbf{r}) \sim i\,\frac{e^{-i\pi/3}\,e^{\alpha_1 x_g e^{5i\pi/6}}e^{iks_g(\mathbf{r})}}{Ai'(-\alpha_1)}\,\frac{\hat{\mathbf{n}}_{sb}\cdot\mathbf{H}^{\mathrm{TM},i}(\mathbf{r}_{sb})}{\hat{\mathbf{n}}_{sb}\cdot\hat{\phi}^i\sin\theta^i} \cdot\left(\frac{\rho_g(\mathbf{r}_{sb})}{\rho_g(\mathbf{r})}\right)^{1/6}\left(\frac{k\rho_g(\mathbf{r})}{2}\right)^{-1/3} \tag{15}$$

where α_1 is the negative of the first zero of the Airy function.

C. Example

In Fig. 2, we have plotted the amplitude of the approximate TE NU current $K_\phi^{\mathrm{TE,\,NU}}(a,\,\phi,\,z)$ for a circular cylinder of radius a with $ka = 60$, $\phi^i = 180°$, and $\theta^i = 90°$ (normal incidence) along with the amplitude of the exact current obtained from the eigenfunction expansion for scattering from a circular cylinder. The expressions from which these plots were made are given in [14] along with the corresponding Fock currents for the parabolic cylinder. The amplitude is discontinuous at the shadow boundary at $\phi = 90°$ because the TE PO current is discontinuous there and, hence, when subtracted from the continuous total current gives a discontinuous NU current. The approximate current is seen to closely fit the exact current except for the ripple behavior of the exact current in the deep shadow region in the vicinity of $\phi = 0°$. This ripple behavior is the result of interference between the dominant creeping waves launched at $\phi = \pm 90°$ both of which are present in the exact eigenfunction expansion of the current, whereas the approximate current in the range $0° \le \phi \le 180°$ contains only the dominant creeping wave launched at $\phi = 90°$.

III. Integrating the Fock Currents to Obtain ILDC's

We will now show how the ILDC's corresponding to the Fock currents, presented in Section II, can be obtained efficiently. The ILDC's for the shadow boundary of a convex cylinder represent the fields radiated by the nonuniform Fock currents on that cylinder. Specifically, the far field, radiated by a strip of thickness dz', which is described by the curve C on the cylinder, is given by

$$d\mathbf{E}^{\mathrm{NU}}(\mathbf{r}) \overset{r\to\infty}{\sim} \frac{dz'\,ik\,e^{ikr}}{4\pi r}\sqrt{\frac{\mu}{\epsilon}}\int_C e^{-ik\hat{\mathbf{r}}\cdot\mathbf{r}_C(s)} \cdot\left[\mathbf{K}^{\mathrm{NU}}(\theta^i,\phi^i,s) - \hat{\mathbf{r}}\,\hat{\mathbf{r}}\cdot\mathbf{K}^{NU}(\theta^i,\,\phi^i,\,s)\right]ds \tag{16}$$

where $\hat{\mathbf{r}}$ is the direction to the far-field observation point, $\mathbf{r}_C(s)$ is the parametric representation of C, and $\mathbf{K}^{\mathrm{NU}}$ is the nonuniform Fock current. In the illuminated region, the curve C is normal to the shadow boundary. In the shadow region, C is the geodesic whose angle with the axial direction is θ^i, as shown in Fig. 1.

In general, it is not possible to evaluate the integral (16) in closed form. However, as we will now demonstrate, an accurate and rapidly calculable approximation to this integral can be obtained.

A. Quadratic Polynomial Approximations of the Amplitude and Phase of the ILDC Radiation Integral

Begin by considering one of the components of the electric field $d\mathbf{E}$ in (16) and write this component as

$$dE(\mathbf{r}) = \int_{s_a}^{s_b} A(s)e^{-iP(s)}\,ds \tag{17}$$

where the amplitude $A(s)$ and the phase $P(s)$ are functions of the angles of incidence and observation. The amplitude and phase functions are determined from the nonuniform current and the far-field Green's function occurring in (16). For convenience, we allow the amplitude $A(s)$ to be complex. Moreover, the expressions in Section II for the Fock currents and the factor $e^{-ik\hat{\mathbf{r}}\cdot\mathbf{r}_C(s)}$ determine the unwrapped phase of the integrand so that the function $P(s)$ is continuous except possibly at the shadow boundary. Thus, the phase function $P(s)$ is *not* restricted to a finite interval of length 2π.

We can divide the integration in (17) into subintervals and have

$$\int_{s_a}^{s_b} A(s)e^{-iP(s)}\,ds = \sum_{j=1}^{n}\int_{s_j}^{s_{j+1}} A(s)e^{-iP(s)}\,ds \tag{18}$$

where $s_1 = s_a$, $s_{n+1} = s_b$, and $s_j < s_{j+1}$. The form of the functions $A(s)$ and $P(s)$ leads one to assume that these functions can be accurately approximated by quadratic

polynomials of s in each of the intervals $s_j < s < s_{j+1}$ when these intervals are chosen appropriately. Hence,

$$\int_{s_j}^{s_{j+1}} A(s)e^{-iP(s)}\,ds \simeq \int_{s_j}^{s_{j+1}} (c_0 s^2 + c_1 s + c_2) \cdot e^{-i(c_3 s^2 + c_4 s + c_5)}\,ds \tag{19}$$

where c_0, c_1, c_2, c_3, c_4, and c_5 are constants independent of s.

These constants will be determined such that the quadratic polynomials fit A and P at the endpoints s_j and s_{j+1} and at the midpoint $s_{j+1/2} = (s_j + s_{j+1})/2$

$$A(s) = c_0 s^2 + c_1 s + c_2, \qquad \text{for } s = s_j, s = s_{j+1/2}, s = s_{j+1} \tag{20}$$

which gives

$$c_0 = 2(s_{j+1} + s_j)\frac{A(s_{j+1}) - A(s_j)}{(s_{j+1} - s_j)^3} + 4\frac{s_{j+1}A(s_{j+1}) - s_j A(s_j)}{(s_{j+1} - s_j)^3} - 4\frac{A(s_{j+1/2})}{(s_{j+1} - s_j)^2} \tag{21}$$

$$c_1 = \frac{A(s_{j+1}) - A(s_j)}{s_{j+1} - s_j} - c_0(s_{j+1} + s_j) \tag{22}$$

and

$$c_2 = \frac{s_{j+1}A(s_j) - s_j A(s_{j+1})}{s_{j+1} - s_j} + c_0 s_j s_{j+1}. \tag{23}$$

Similarly,

$$P(s) = c_3 s^2 + c_4 s + c_5, \qquad \text{for } s = s_j,\ s = s_{j+1/2}, s = s_{j+1} \tag{24}$$

and we find that c_3, c_4, and c_5 are given by (21)–(23), respectively, with A replaced by P. These expressions for the constants c_0, c_1, c_2, c_3, c_4, and c_5 are well behaved for all functions A and P that are continuous in the interval $s_j < s < s_{j+1}$. In principle, we could let $P(s)$ be continuous for all s except at the shadow boundary. However, in practical calculations we permit $P(s)$ to have discontinuities that are multiples of 2π at the points s_j.

In the Appendix, we have shown how the integral on the right side of (19) can be evaluated in closed form in terms of the Fresnel function. Thus, the ILDC's are expressed as a finite summation involving the Fresnel function and the values of the amplitude and the unwrapped phase of the integrand in (16) evaluated at the points s_j.

B. Numerical Verification of the Quadratic Approximations

We will now use a numerical example to verify the quadratic approximation of the phase and amplitude in (19). We consider the far field radiated by the NU currents on the circular cylinder shown in Fig. 3. The incident field is a plane TE wave with $H_z^i = e^{ikx}$ and only the NU currents in the angular region $0 \le \phi \le \pi$ will be taken into account. The magnetic far field for this NU current can be written as $H_z^{\mathrm{NU,\,TE}}(\mathbf{r}) = \mathcal{F}^{\mathrm{NU,\,TE}}(\phi)e^{ikr}/\sqrt{kr}$, where the far-field

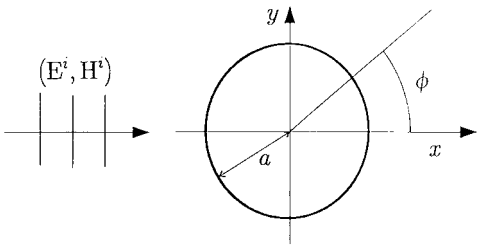

Fig. 3. Circular cylinder illuminated by a TE plane wave.

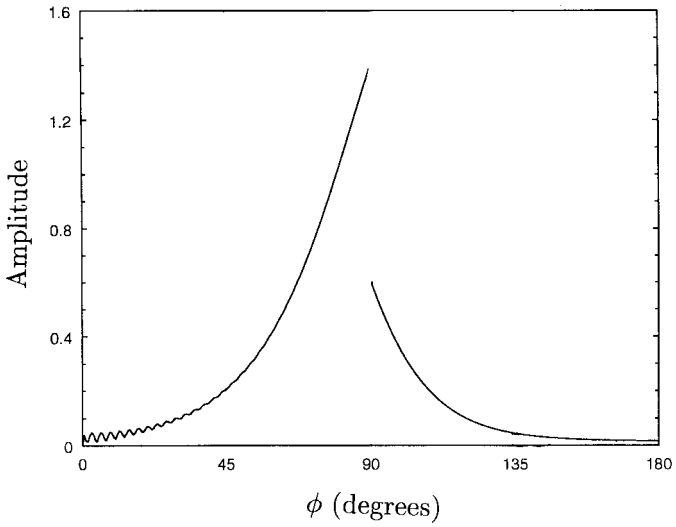

Fig. 4. Amplitude of the exact nonuniform TE current on circular cylinder for $ka = 60$.

pattern is given by

$$\mathcal{F}^{\mathrm{NU,TE}}(\phi) = \int_{s_a}^{s_b} A(s)e^{-iP(s)}ds \tag{25}$$

with $s_a = 0$, $s_b = \pi$,

$$A(s) = -\frac{ka}{\sqrt{8\pi}}|K_\phi^{\mathrm{NU,\,TE}}(s)|\cos(\phi - s) \tag{26}$$

and

$$P(s) = ka\cos(\phi - s) - \mathrm{Phase}(K_\phi^{\mathrm{NU,\,TE}}(s)) \tag{27}$$

where $\mathrm{Phase}(K_\phi^{\mathrm{NU,\,TE}}(s))$ is continuous (i.e., *not* modulo 2π) apart from the discontinuity at the shadow boundary.

The amplitude and unwrapped phase of the NU current are shown in Figs. 4 and 5, respectively, for $ka = 60$. Notice that both the unwrapped phase and the amplitude of the NU current have discontinuities at the shadow boundary and that the unwrapped phase is almost linear on the shadow side.

Figs. 6 and 7 show the exact values and the quadratic approximations of $A(s)$ and $P(s)$ for $\phi = 0°$. The number of segments n in (18) is six and $s_j = \pi(j-1)/6$ so the shadow region $0 \le s < \pi/2$, as well as the illuminated region $\pi/2 \le s \le \pi$, is divided into three subregions. Thus, the length of the subintervals is 5λ. To better illustrate the accuracy of the quadratic phase approximation, we have introduced discontinuities in the phase at the endpoints s_j. We see that the quadratic phase approximation is excellent for both

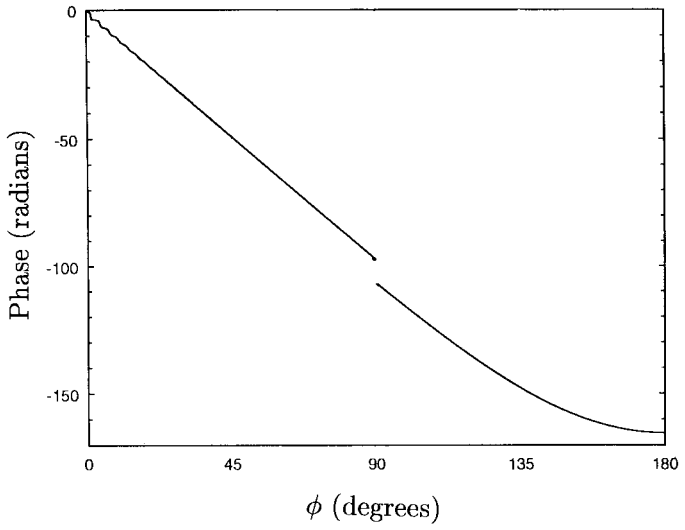

Fig. 5. Phase of the exact nonuniform TE current on circular cylinder for $ka = 60$.

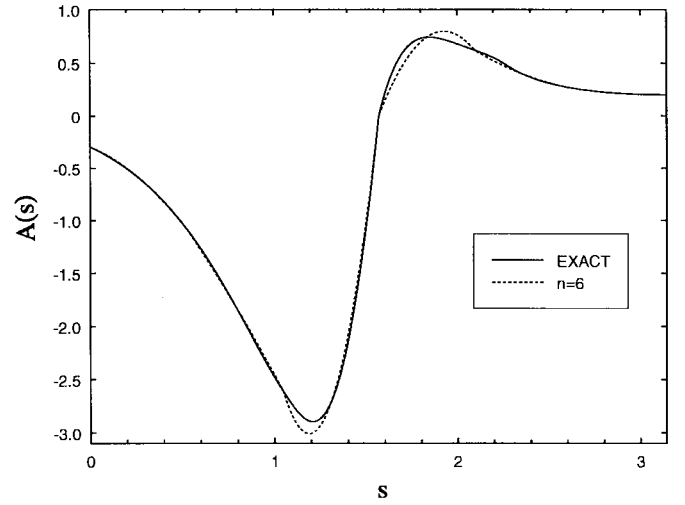

Fig. 6. Exact values and quadratic approximation of $A(s)$ for $n = 6$, $\phi = 0°$, and $ka = 60$. The endpoints are $s_j = \pi(j-1)/6$.

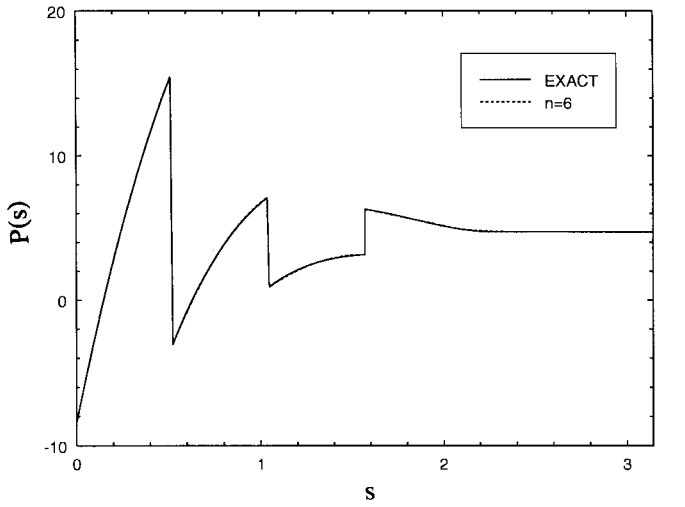

Fig. 7. Exact values and quadratic approximation of $P(s)$ for $n = 6$, $\phi = 0°$, and $ka = 60$. The endpoints are $s_j = \pi(j-1)/6$.

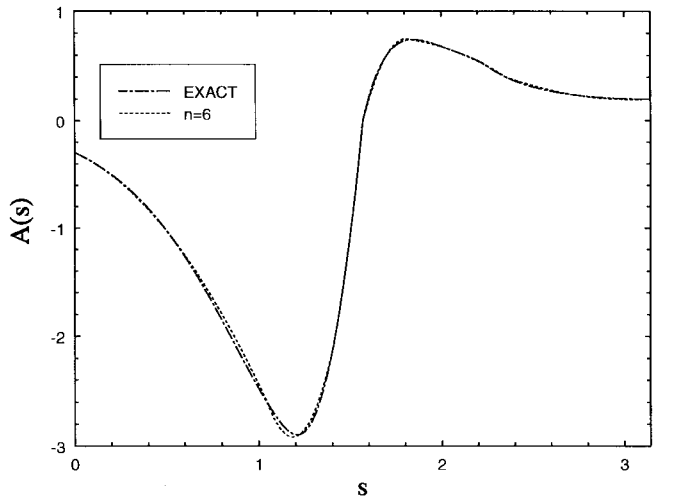

Fig. 8. Exact values and quadratic approximation of $A(s)$ for $n = 6$, $\phi = 0°$, and $ka = 60$. The endpoints are $s_1 = 0$, $s_2 = 60°$, $s_3 = 80°$, $s_4 = 90°$, $s_5 = 105°$, $s_6 = 135°$, and $s_7 = 180°$.

these angles of observation, but that the quadratic amplitude approximation deviates somewhat from the exact amplitude.

The quadratic amplitude approximation can be improved by using unequal spacing with a greater density of points taken in the region of s that contributes most strongly to the far field at ϕ. As an example, this is done in Fig. 8 for $\phi = 0$ where the endpoints are given by $s_1 = 0$, $s_2 = 60°$, $s_3 = 80°$, $s_4 = 90°$, $s_5 = 105°$, $s_6 = 135°$, and $s_7 = 180°$. The quadratic approximation is clearly better in Fig. 8 than in Fig. 6 with equal spacing. Future work could determine the optimal set of endpoints s_j as a function of the far-field angle of observation. By making these endpoints depend on the far-field angle, one could probably increase the accuracy of the computed ILDC's and, at the same time, reduce the number of segments.

Having demonstrated the validity of the quadratic approximations for the amplitude $A(s)$ and phase $P(s)$, we can now calculate the far field that results from these approximations using (18) and (19). For the above example of a TE plane wave incident on a circular cylinder, the NU far-field pattern is shown in Figs. 9 and 10. We notice that, except in the region around $\phi = 20°$, the results obtained with $n = 4$ are very accurate. It is almost impossible to distinguish the exact result from the result obtained with $n = 8$ and we conclude that for $ka = 60$ it is sufficient to use $n = 6$ equally spaced endpoints.

The numerical examples in this section show that with the integration technique presented in Section III-A, one can accurately compute the radiated fields using segments as large as 5λ. This is a significant improvement over standard current integrations that usually use segments of the order of $\lambda/6$.

IV. The Use of the ILDC's for a 3-D Scatterer

In this section, we show how the ILDC's for a convex cylinder are applied to calculate the scattered far field of a 3-D scatterer. In applications, the PO field will generally be known and what is desired is the scattered field due to the NU currents

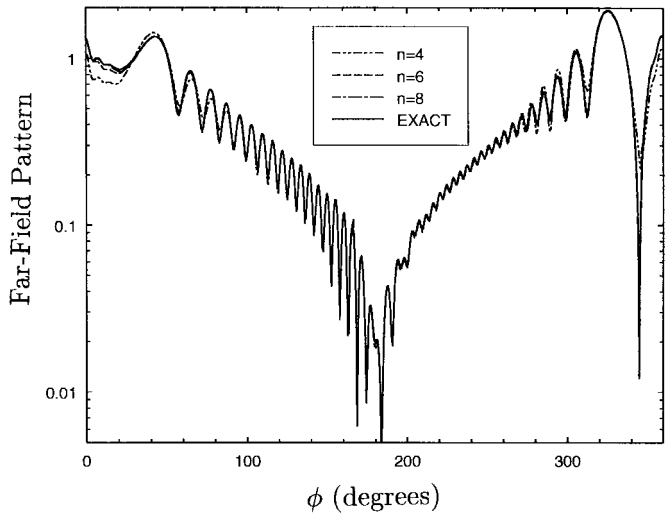

Fig. 9. Exact and approximate NU TE far-field pattern for $ka = 60$ and $n = 4$, $n = 6$, and $n = 8$. The endpoints are $s_j = \pi(j-1)/n$.

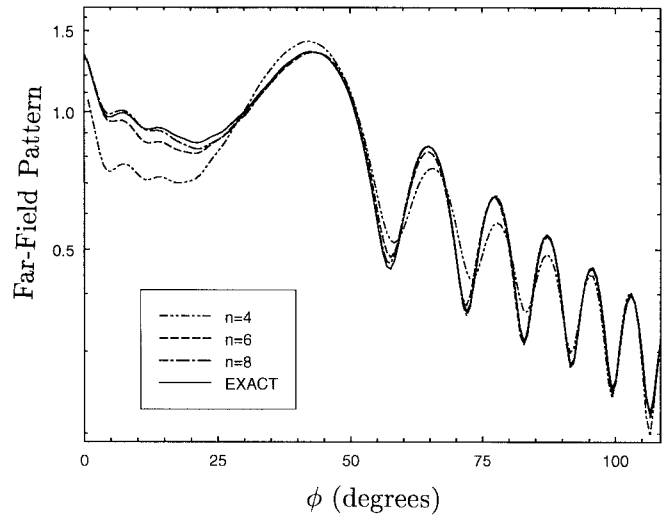

Fig. 10. Exact and approximate NU TE far-field pattern for $ka = 60$ and $n = 4$, $n = 6$, and $n = 8$. The endpoints are $s_j = \pi(j-1)/n$. Only the angular region $0 < \phi < 110^\circ$ is shown.

on the 3-D scatterer in the vicinity of its shadow boundary. The total scattered field is then obtained by adding the NU scattered field to the PO field. Consider a 3-D scatterer with a smoothly varying radius of curvature illuminated by a plane wave (see Fig. 11). The illuminated and shadowed portions of the surface are separated by the shadow boundary curve on the surface of the scatterer. Consider a point P on the shadow boundary and generate a curve C on the surface of the scatterer through P motivated by the behavior of the currents on the surface. In the shadow region, C is the geodesic emanating from P in the direction of the illuminating plane wave—the curve followed by the currents—while in the illuminated region where the currents are determined locally, C is simply the intersection of the surface with the plane through P perpendicular to the shadow boundary. A 2-D convex cylindrical (in general, not circular-cylindrical) surface can then be generated by passing straight lines (generators) through each point on C parallel to

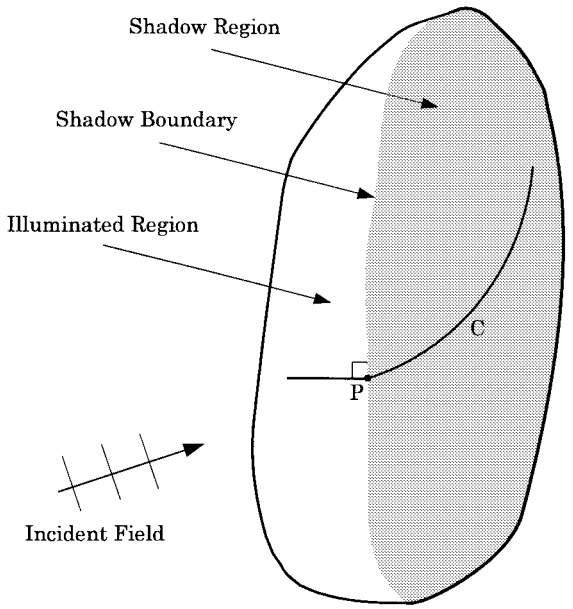

Fig. 11. Three-dimensional scatterer illuminated by a plane wave.

the shadow boundary at P. Now generate a curve C' through P on the cylindrical surface in the same way that C was generated on the surface of the 3-D scatterer. Assume that the radius of curvature of the 3-D scatterer is large in the direction parallel to the shadow boundary at P for points on the geodesic part of C, especially in the vicinity of P. Then the geodesic portion of C in the vicinity of P will be closely approximated by the geodesic portion of C' (a generalized helical curve on the convex cylindrical surface making a constant angle with its generators), and the ILDC's of the cylindrical surface at P will be a good approximation to the fields radiated by the NU currents on a differential strip of the 3-D scatterer's surface containing C. The procedure for obtaining the ILDC's corresponding to the point P on the shadow boundary of the 3-D scatterer is repeated for all points on the shadow boundary, and the ILDC's then integrated along the shadow boundary to obtain an approximation to the far field radiated by the NU currents on the 3-D scatterer.

It should be noted that a creeping wave geodesic on the surface of the actual scatterer will, in general, diverge from the corresponding helical creeping wave geodesic on the approximating convex cylinder surface as the distance from the launching shadow boundary point increases. However, the exponential decay of the creeping waves (8), (15) insures that the major contribution to the diffracted far field comes from the current on the portion of the geodesic close to the shadow boundary. Here, the generalized helical geodesic can be expected to be a good approximation to the actual creeping wave geodesic, especially if, as assumed, the radius of curvature of the actual 3-D scatterer is large in the direction parallel to the shadow boundary for points on the geodesic close to the launching shadow boundary point. An important consequence of this concentration of the creeping wave current in the vicinity of the shadow boundary is that the major ILDC contribution to the far field is in the forward direction since the field in this region can be viewed as due to the shedding

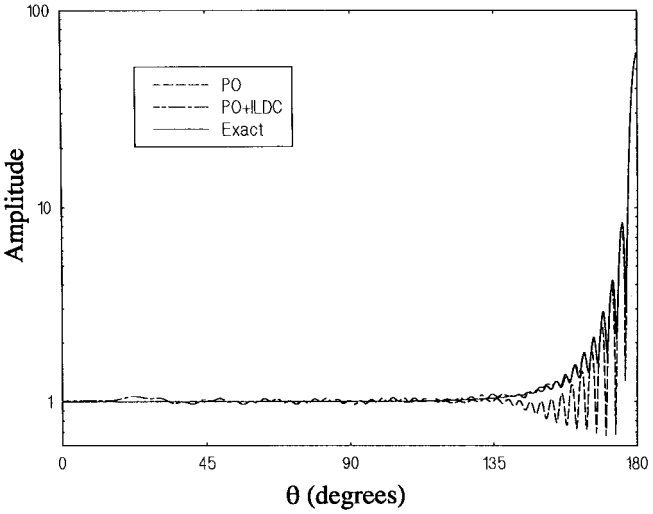

Fig. 12. Amplitude of scattered H-plane far field of sphere $ka = 60$ illuminated by a plane wave; $0° \leq \theta \leq 180°$.

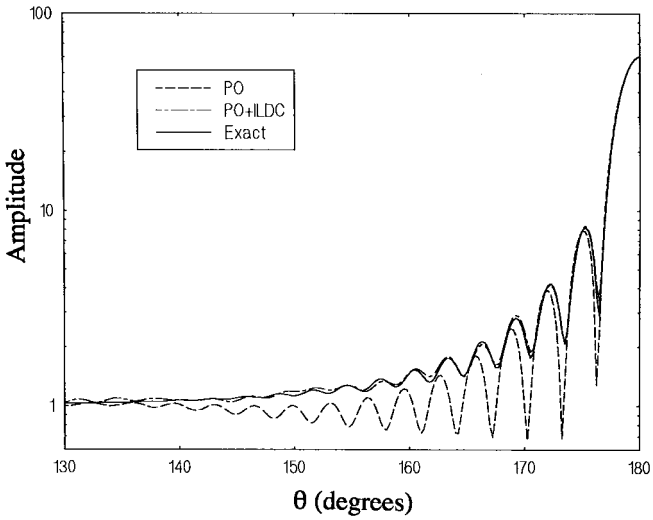

Fig. 13. Amplitude of scattered H-plane far field of sphere $ka = 60$ illuminated by a plane wave; $130° \leq \theta \leq 180°$.

of the creeping waves along rays tangential to the scatterer at points close to the shadow boundary.

A. Calculation of the Fields Scattered by a Sphere

As an application of the NU ILDC's for the shadow boundary of the PEC circular cylinder, we calculated the far field of a PEC sphere illuminated by a plane wave by adding the integral of the ILDC for a cylinder to the PO field of the sphere and compared the result to the exact scattered far field of the sphere as obtained from the Mie series solution. The sphere of radius a is assumed centered at the origin of a Cartesian coordinate system and illuminated by a plane wave propagating from above in the negative z direction. The shadow boundary of the sphere is thus a circle of radius a in the $z = 0$ plane. A circular cylinder of radius a enclosing the sphere, whose axis lies in the plane $z = 0$, will be tangent to the sphere along the circle of radius a, normal to the cylinder axis, with its center at the origin. Hence, a strip of the sphere's surface of constant equal width on either side of the meridian defined by $\phi =$ constant coincides in the limit, as the width of the strip shrinks to zero with an azimuthal differential strip of surface of the enclosing cylinder. As the cylinder is rotated around the z axis, the entire surface of the sphere is obtained. Thus, the far field of the sphere can be obtained by adding the integral of the NU-current ILDC of the cylinder to the PO far field of the sphere, as the cylinder axis is rotated from $\phi = 0$ to $\phi = 2\pi$. (It should be noted that an error is introduced in this approximation procedure by the fact that the differential strips of cylinder surface overlap in the vicinity of the poles of the sphere as the cylinder is rotated. This overlap is concentrated in the "polar" regions of the sphere, however, and if the radius of the sphere is large, the NU currents will decay rapidly away from the shadow boundary so that the error attributable to the overlap of the differential strips can be expected to be small.)

In Fig. 12, we show the scattered H-plane far field for a sphere of size $ka = 60$ illuminated by a plane wave obtained by the method of ILDC's, along with the exact field obtained from the Mie series. The back and forward scatter directions correspond to $\theta = 0°$ and $\theta = 180°$, respectively. The detail of Fig. 12 for $130° \leq \theta \leq 180°$ is shown in Fig. 13. It can be seen that a significant improvement upon the accuracy of the PO scattered field is obtained by adding the integral of the circular cylinder NU current ILDC to the PO field of the sphere. A similar result was obtained for the E-plane scattered far-field pattern. Calculations for spheres smaller than $ka = 60$ have shown that the ILDC's significantly enhance the accuracy of the PO far field for spheres as small as $ka = 20$.

V. Conclusions

The nonuniform currents excited in the vicinity of the shadow boundary of a PEC object can contribute significantly to the total scattered far field of the object. The method of ILDC's is an important technique for calculating this NU field, which, added to the PO field, gives a considerably more accurate approximation to the total far field than does the PO far field alone. The approach taken in this paper to obtain ILDC's for the shadow boundary of a PEC 2-D convex cylinder of general cross section is to integrate the product of the free-space Green's function and the NU currents over a strip of surface of the 2-D cylinder of differential width, transverse to the shadow boundary. Accurate and rapidly calculable Fock approximations to the NU currents are obtained and used. The integration required to obtain the ILDC's is itself performed rapidly by using quadratic polynomial approximations of both the amplitude and unwrapped phase of the integrand of the radiation integral, thereby enabling the integration to be performed in closed form involving Fresnel functions. Examples are given of the approximations of both the NU currents and the integrand of the radiation integral. As an application of this method of obtaining ILDC's for convex PEC cylinders, the ILDC's of a PEC circular cylinder are obtained and integrated over the shadow boundary of a PEC sphere illuminated by a plane wave to obtain the NU current far field. This field, added to the PO far field, is shown to considerably improve upon the accuracy of the

PO approximation of the exact total scattered far field of the sphere.

APPENDIX

A. Closed-Form Expressions for an Integral

Here we present closed-form expressions for the integral

$$I(c_0, c_1, c_2, c_3, c_4, c_5, a, b) = \int_a^b (c_0 s^2 + c_1 s + c_2) e^{-i(c_3 s^2 + c_4 s + c_5)}\, ds \tag{28}$$

occurring in (19). We assume that c_0, c_1, and c_2 are complex and that c_3, c_4, c_5, a, and b are real.

Case I $(c_3 > 0)$*:* Integration by parts shows that

$$\begin{aligned} I(c_0, c_1, c_2, c_3, c_4, c_5, a, b) &= \frac{ic_0}{2c_3}\left[\left(b + \frac{c_4}{2c_3}\right)e^{-i(c_3 b^2 + c_4 b + c_5)} - \left(a + \frac{c_4}{2c_3}\right)e^{-i(c_3 a^2 + c_4 a + c_5)}\right] \\ &\quad + \frac{i}{2c_3}\left(c_1 - \frac{c_0 c_4}{c_3}\right)\left[e^{-i(c_3 b^2 + c_4 b + c_5)} - e^{-i(c_3 a^2 + c_4 a + c_5)}\right] \\ &\quad + \left(\frac{c_0}{2ic_3} - \frac{c_1 c_4}{2c_3} + c_2 + \frac{c_0 c_4^2}{4c_3^2}\right)\Lambda \end{aligned} \tag{29}$$

where

$$\Lambda = \sqrt{\frac{\pi}{2c_3}}\, e^{-i[c_5 - c_4^2/(4c_3)]}[\Omega(x_b) - \Omega(x_a)] \tag{30}$$

$$x_a = \sqrt{\frac{2c_3}{\pi}}\left\{a + \frac{c_4}{2c_3}\right\}, \quad x_b = \sqrt{\frac{2c_3}{\pi}}\left\{b + \frac{c_4}{2c_3}\right\} \tag{31}$$

and

$$\Omega(x) = \int_0^x e^{-i\pi t^2/2}\, dt \tag{32}$$

is a Fresnel function. When $|x_a|$ and $|x_b|$ are large, one can substitute the large-argument approximation for the Fresnel function [16]

$$\Omega(x) \sim \operatorname{sign}(x)\frac{1-i}{2} + \left[\frac{i}{\pi x} - \frac{1}{\pi^2 x^3} - \frac{3i}{\pi^3 x^5} + O(x^{-7})\right] \cdot e^{-i\pi x^2/2}, \quad |x| \to \infty \tag{33}$$

into (30) to get

$$\Lambda = \frac{i}{\sqrt{2\pi c_3}}\left[\left(\frac{1}{x_b} + \frac{i}{\pi x_b^3} - \frac{3}{\pi^2 x_b^5}\right)e^{-i(c_3 b^2 + c_4 b + c_5)} - \left(\frac{1}{x_a} + \frac{i}{\pi x_a^3} - \frac{3}{\pi^2 x_a^5}\right)e^{-i(c_3 a^2 + c_4 a + c_5)}\right]. \tag{34}$$

Numerical calculations show that it is advantageous to use (34) when $|x_a| > 10$ and $|x_b| > 10$. For $|x_a| \le 10$ or $|x_b| \le 10$, the routine "fresnel" of numerical recipes [17, pp. 248–250] can be used.

Case II $(c_3 < 0)$*:* The integral can in this case be obtained from

$$I(c_0, c_1, c_2, c_3, c_4, c_5, a, b) = [I(c_0^*, c_1^*, c_2^*, -c_3, -c_4, -c_5, a, b)]^* \tag{35}$$

where $*$ indicates complex conjugation. The integral on the right side of (35) can be computed by the formulas given in Case I above.

Case III $(0 < |c_3| \ll 1)$*:* In this case, it is advantageous to obtain I from

$$I(c_0, c_1, c_2, c_3, c_4, c_5, a, b) = I(c_0, c_1, c_2, 0, c_4, c_5, a, b) + c_3 \frac{\partial I}{\partial c_3}(c_0, c_1, c_2, 0, c_4, c_5, a, b) \tag{36}$$

where

$$\frac{\partial I}{\partial c_3}(c_0, c_1, c_2, 0, c_4, c_5, a, b) = -i\int_a^b s^2(c_0 s^2 + c_1 s + c_2)\, e^{-i(c_4 s + c_5)} ds. \tag{37}$$

The integral can be easily evaluated in closed form by integrating by parts or, more simply, by using a symbolic-integration computer program.

Case IV $(c_3 = 0,\ c_4 \neq 0)$*:* A straightforward calculation shows that

$$\begin{aligned} I(c_0, c_1, c_2, 0, c_4, c_5, a, b) &= \left[-\frac{c_0 b^2 + c_1 b + c_2}{ic_4} + \frac{2c_0 b + c_1}{c_4^2} + \frac{2c_0}{ic_4^3}\right]e^{-i(c_4 b + c_5)} \\ &\quad - \left[-\frac{c_0 a^2 + c_1 a + c_2}{ic_4} + \frac{2c_0 a + c_1}{c_4^2} + \frac{2c_0}{ic_4^3}\right]e^{-i(c_4 a + c_5)}. \end{aligned} \tag{38}$$

Case V $(c_3 = 0,\ c_4 = 0)$*:* A straightforward calculation shows that

$$I(c_0, c_1, c_2, 0, 0, c_5, a, b) = \left[\tfrac{1}{3}c_0(b^3 - a^3) + \tfrac{1}{2}c_1(b^2 - a^2) + c_2(b - a)\right]e^{-ic_5}. \tag{39}$$

Equation (24) implies that the quantities $e^{-i(c_3 a^2 + c_4 a + c_5)}$ and $e^{-i(c_3 b^2 + c_4 b + c_5)}$, occurring in many of the expressions of this section, simply equal $e^{-iP(a)}$ and $e^{-iP(b)}$, respectively.

REFERENCES

[1] P. Y. Ufimtsev, *Method of Edge Waves in the Physical Theory of Diffraction.* Moscow, Russia: Sovyetskoye Radio, 1962 (Engl. transl. available from Nat. Tech. Inform. Serv., Springfield, VA 22161 USA; #AD733203.)

[2] K. M. Mitzner, *Incremental Length Diffraction Coefficients,* Tech. Rep. no. AFAL-TR-73-296, Apr. 1974 (available Nat. Tech. Inform. Serv., Springfield VA 22161 USA; #AD918861).

[3] A. Michaeli, "Equivalent edge currents for arbitrary aspects of observation," *IEEE Trans. Antennas Propagat.,* vol. AP-32, pp. 252–258, Mar. 1984; Corrections *IEEE Trans. Antennas Propagat.,* vol. AP-33, p. 227, Feb. 1985.

[4] E. F. Knott, "The relationship between Mitzner's ILDC and Michaeli's equivalent currents," *IEEE Trans. Antennas Propagat.,* vol. AP-33, pp. 112–114, Jan. 1985.

[5] R. A. Shore and A. D. Yaghjian, "Incremental diffraction coefficients for planar surfaces," *IEEE Trans. Antennas Propagat.,* vol. 36, pp. 55–70, Jan. 1988; Corrections *IEEE Trans. Antennas Propagat.,* vol. 37, p. 1342, Oct. 1989.
[6] A. D. Yaghjian, R. A. Shore, and M. B. Woodworth, "Shadow boundary incremental length diffraction coefficients for perfectly conducting smooth, convex surfaces," *Radio Sci.,* vol. 31, pp. 1681–1695, Nov./Dec. 1996.
[7] T. B. Hansen and A. D. Yaghjian, "Incremental diffraction coefficients for cylinders of arbitrary cross section: Application to diffraction from ridges and channels in perfectly conducting surfaces," in *IEEE Antennas Propagat. Soc. Symp. Dig.,* Univ. Western Ontario, London, ON, Canada, June 1991, pp. 794–797.
[8] R. A. Shore and A. D. Yaghjian, "A comparison of two incremental diffraction coefficients for convex perfectly electrically conducting cylinders," in *Int. Symp. Electromagn. Theory, Int. Union Radio Sci. (URSI),* Aristotle Univ., Thessaloniki, Greece, May 1998, pp. 4–6.
[9] V. A. Fock, *Electromagnetic Diffraction and Propagation Problems.* Oxford, U.K.: Pergamon, 1965.
[10] L. N. Medgyesi-Mitschang and D. L. Wang, "Hybrid solutions for scattering from perfectly conducting bodies of revolution," *IEEE Trans. Antennas Propagat.,* vol. AP-31, pp. 570–583, July 1983.
[11] G. T. Ruch, Ed., *Radar Cross Section Handbook.* New York: Plenum, 1970, vol. 1.
[12] D. P. Bouche, F. A. Molinet, and R. Mittra, "Asymptotic and hybrid techniques for electromagnetic scattering," *Proc. IEEE,* vol. 81, pp. 1658–1684, Dec. 1993.
[13] T. B. Hansen and R. A. Shore, "The currents on a cylinder illuminated by a general plane wave," *IEEE Trans. Antennas Propagat.,* vol. 43, pp. 1464–1465, Dec. 1995.
[14] ———, "Incremental length diffraction coefficients for the shadow boundary of a general cylinder," Rome Lab. Rep. RL-TR-97-151, July 1997.
[15] J. J. Bowman, T. B. A. Senior, and P. L. E. Uslenghi, *Electromagnetic and Acoustic Scattering by Simple Shapes.* Amsterdam, The Netherlands: North-Holland, 1969.
[16] M. Abramowitz and I. A. Stegun, *Handbook of Mathematical Functions.* New York: Dover, 1972 (9th printing).
[17] W. H. Press, S. A. Teukolsky, W. T. Vetterling, and B. P. Flannery, *Numerical Recipes in Fortran.* New York: Oxford Univ. Press, 1992.

Thorkild B. Hansen (S'91–M'91) was born in Odense, Denmark, on January 26, 1965. He received the M.S. and Ph.D. degrees from the Technical University of Denmark, Lyngby, in 1989 and 1991, respectively.

From 1992 to 1997, he was with Rome Laboratory, Hanscom AFB, MA. In 1997 he joined Schlumberger-Doll Research, Ridgefield, CT.

Dr. Hansen has won two best-paper awards for papers published in IEEE TRANSACTIONS ON ANTENNAS AND PROPAGATION, the 1992 R.W.P. King Prize Paper Award for a paper on corner diffraction, and the 1995 S.A. Schelkunoff Prize Paper Award for a paper on near-field scanning. He is a member of the Optical Society of America, the American Association for the Advancement of Science, and URSI Commission B.

Robert A. Shore (M'93–SM'96) was born in Brooklyn, NY, in 1936. He received the B.A. degree from Amherst College, Amherst, MA, and the Ph.D. degree from Harvard University, Cambridge, MA, (both in applied mathematics) in 1957 and 1968, respectively.

From 1959 to 1969, he worked at the Air Force Cambridge Research Laboratory, Cambridge, MA, in the fields of diffraction theory and partial coherence. From 1970 to 1975 he was with Israel Aircraft Industries, Yahud, Israel, and from 1975 to 1980 he was with Energy Resources Co., Cambridge, MA. Since 1980 he has worked at Rome Laboratory (now Air Force Research Laboratory), Hanscom AFB, MA, in the areas of adaptive antennas, reflector antennas, and high-frequency diffraction theory.

Dr. Shore is a member of URSI Commission B and the Electromagnetics Academy.